A Novel Contra-Rotating Power Split Transmission System for Wind Power Generation and Its Dual MPPT Control Strategy

Xiang Luo and Shuangxia Niu, *Member, IEEE*

***Abstract*—This paper proposes a new brushless contra-rotating power split transmission (CR-PST) system for the direct-drive wind power generation. The core element of this system is a doubly fed dual-rotor flux-modulation permanent magnet machine, which has two contra-rotating rotors connected with two wind blades to absorb the wind energy, and two sets of stator windings to realize torque split between the two shafts. This proposed CR-PST system has compact structure and bidirectional flux-modulation design, as well as increased wind power conversion efficiency. Compared with the conventional wind turbine system, which can only work with single maximum power point tracking (MPPT) control strategy, the proposed CR-PST system can collect increased wind energy with dual MPPT method for the given wind speed. Time-stepping finite-element method is used to analyze the steady and dynamic performance of the proposed system and the control strategy is verified by experiments and simulation results.**

***Index Terms*—Contra-rotating, dual-rotor machine, magnetic flux modulation, maximum power point tracking (MPPT) control, power split, wind power generator.**

I. Introduction

WIND energy is completely clean, inexhaustible, sustainable, and requiring little maintenance, the collection of which is being increasingly investigated at the worldwide level. Hitherto, single-rotor generation system is commonly used for wind energy conversion [1], [2]. However, single-rotor systems are only able to convert at most about 59% of the total wind stream energy into useful electric energy [3]. To increase the energy-extraction efficiency, contra-rotating wind turbine (CRWT) generation system is developed and laboratory tests indicate that using a contra-rotating rotor system could increase power conversion efficiency by 40% than a single-rotor system [4].

The research of contra-rotating system can be dated back as early as 1940s, and last till nowadays [5], [6]. Contra-rotating system was studied mainly as a propeller for aircraft propulsion and lift, as well as marine propulsion. The system has shown a lot of advantages compared with single-rotor systems, such as the propeller-induced heeling moment can be compensated; more power can be transmitted for a given propeller radius, and the propeller efficiency can be increased by recovering energy from the tangential (rotational) flow from the leading propeller, etc. In recent years, some researchers intended to introduce the contra-rotating system into wind power generation, and some of the achievements have been reached [7]–[9]. Both the hydromechanics and the generator design of the contra-rotating system are all the recent research hotspots.

In the existing CRWT practices, usually two separate electric generators are combined together to fulfill the requirements of the contra-rotating system [3]. However, this kind of design is complicated and bulky in size. Another design has only one generator involved in the contra-rotating system, but the stator armature and permanent magnets (PMs) need to rotate in opposite directions. Therefore, additional slip ring assembly and brushes are required, which leads to maintenance problem and low reliability, as shown in Fig. 1 [8].

To overcome above problems, some researchers introduce the continuously variable transmission (CVT) system into the contra-rotating system [10]–[15]. This technique, which is initially being used in hybrid electric vehicles, can realize flexible control of torque and transmission speed. With the CVT-based power split design for wind energy conversion system, the machine size of the generator can be reduced and the large capacity

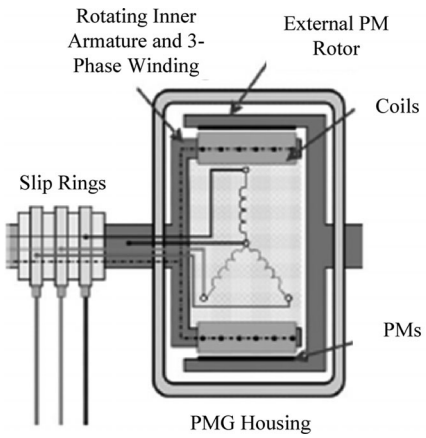

Fig. 1. Dual rotor generator for contra-rotating wind system with slip ring [8].

Manuscript received May 5, 2016; revised August 1, 2016 and October 26, 2016; accepted November 4, 2016. Date of publication November 15, 2016; date of current version April 24, 2017. This work was supported by the Research Grand Council, Hong Kong Special Administrative Region, China, under projects PolyU 152130/14E. Recommended for publication by Associate Editor Y. W. Lei. *(Corresponding author: Shuangxia Niu.)*

X. Luo is with the Department of Electrical Engineering, The Hong Kong Polytechnic University, Hong Kong, and is also with the Department of Electrical Engineering, Shanghai Jiao Tong University, Shanghai, China (e-mail: maskluo@sjtu.edu.cn).

S. Niu is with the Department of Electrical Engineering, The Hong Kong Polytechnic University, Hong Kong (e-mail: eesxniu@polyu.edu.hk).

Color versions of one or more of the figures in this paper are available online at http://ieeexplore.ieee.org.

Digital Object Identifier 10.1109/TPEL.2016.2629021

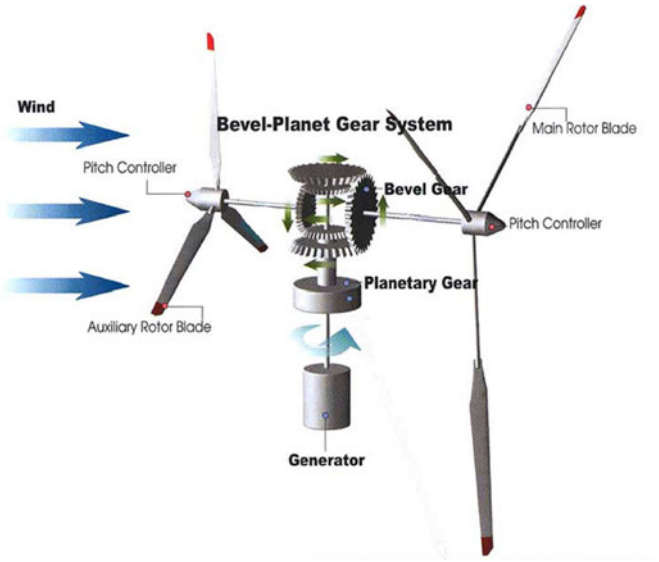

Fig. 2. Planetary gear system-based contra-rotating system [14].

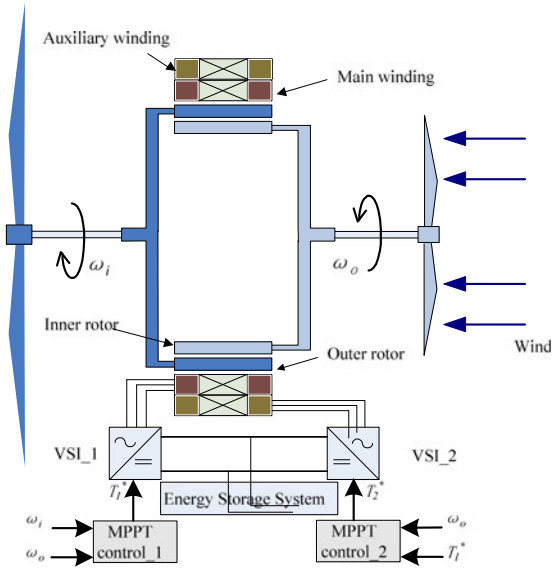

Fig. 3. Proposed CR-PST system for wind power generation.

power electronic converter from the generator to the grid is not needed [12], [13].

In [14], a bevel-planetary gear box-based power split CVT system is applied for CRWT system to increase the wind energy absorption rate as well as realize the torque split and combination, as shown in Fig. 2. The combined torque from contra-rotating rotors is transmitted to the sun gear which is finally connected with a vertical axis wind turbine system to generate electricity. From their research, improved aerodynamic efficiency is attainable. However, the mechanical gearbox-based system suffers from acoustic noise, maintenance problem, and low reliability, and the fixed gear ratio of the gear system makes the torque split ratio on the two shafts constant, which results in the maximum power point tracking (MPPT) on both shafts impossible.

In this paper, the proposed brushless contra-rotating power split transmission (CR-PST) system is proposed to replace the bevel-planetary gear box-based power split CVT system. There is no mechanical gear boxes involved and also no brushes or slip rings. Therefore, mechanical problems can be avoided and there is also minimum acoustic noise. The core element of the proposed system is a doubly fed dual-rotor flux-modulation PM (DDF-PM) machine. Its operation principle is based on magnetic gears (MGs) effect, which utilizes the magnetic flux-modulation principle to transmit the torque and speed without mechanical contact [16]. By introducing the bidirectional flux modulation into the contra-rotating wind generation system, the wind power absorbed by the two contra-rotating wind blades can be combined together and transmitted to the stator windings. The steady and dynamic performances of the proposed machine are simulated by a time-stepping finite element method. Since electromagnetic torque produced by the stator windings can be split to individual rotors, dual MPPT control strategy can be realized to maximize the wind power extraction. The prototype of the best design is fabricated and the experimental results verify the validity and effectiveness of this proposed design and dual MPPT control strategy.

II. System Configuration and Working Principle

A. CR-PST System

As shown in Fig. 3, in the proposed CR-PST system, the core element of the system is a DDF-PM machine, in which the outer rotor serves as the main rotor and is connected with main wind turbine and the inner rotor is connected with auxiliary wind turbine to compensate for the wind energy absorption. Since these rotors rotate in opposite directions, due to the relative angular speeds and also based on the flux-modulation theory, the induced frequency in the main winding is almost doubled, which is desired for wind power generation system. The pole pair number of the outer rotor PM is designed to be equal with that of the auxiliary windings, so that the torque production on the outer rotor can be controlled with the auxiliary winding. While caused by the main winding, the torque distribution on the inner and outer rotor is according to a fixed gear ratio, which is determined by the pole pair number of the inner and outer rotor PMs. Since the torques of dual rotors can be flexibly controlled with the main and auxiliary winding, dual MPPT control strategy can be realized to maximize the wind energy conversion. The system also consists of a dual-inverter system, which includes two sets of voltage source inverters (VSIs), and a battery charging system. The dual-invertor system is connected with the main winding and auxiliary winding, respectively, to realize the dual MPPT control.

The proposed CR-PST system has following advantages:

1) the CRWT can extract extra wind power, which is the main advantage of the CRWT generation system compared to a single-rotor wind generation system;
2) high-energy conversion rate due to a high angular relative velocity of the rotating magnetic field in the air gap. Therefore, the structure is compact,

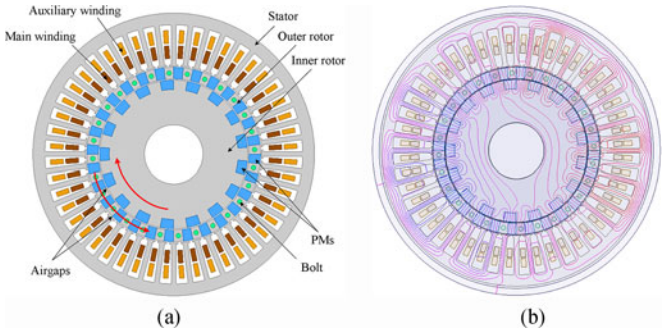

Fig. 4. Proposed DDF-PM machine. (a) Structure of the machine. (b) Flux line distribution.

TABLE I
SPECIFICATIONS OF THE DDF-PM MACHINE

Quantity	Value
Outer radius of stator	108.0 mm
Inner radius of stator	74.7 mm
Outer airgap length	1.0 mm
Inner airgap length	1.0 mm
Radial length of outer rotor	6.1 mm
PM length of inner rotor	15.8 mm
PM pole number in outer rotor	28
PM pole number in inner rotor	17
Main winding pole pair number	11
Auxiliary winding pole pair number	28
Stator slot number	48
Turn number of main winding	30
Turn number of auxiliary winding	30
Stack length	65 mm
Stator and rotor core material	M19_24G
Magnetic remanence	1.2 T
Inner Rotor Rated Torque	20 N·m
Inner Rotor Rated Power	600 W
Outer Rotor Rated Torque	30 N·m
Outer Rotor Rated Power	900 W

3) no slip rings and brushes as no armature windings on rotors, no gear box and reduced maintenance problem and improved reliability;
4) dual MPPT control strategy can be used to optimize the wind energy conversion.

B. Machine Structure

As the core element of the CR-PST system, DDF-PM machine consists of one stator and two rotors. The structure of the proposed machine and its full-load flux line distribution are as shown in Fig. 4. The outer rotor is composed of alternatively arranged 28 pieces of PMs and modulation poles. Similarly, there are 17 pieces of PMs and modulation poles alternatively inset in the inner rotor. The outer rotor rotates in an anti-clockwise direction, while the inner rotor rotates in the opposite direction. The main winding with the pole pair of 11 and the auxiliary winding with the pole pair of 28 are housed in the stator. The specifications of the machine are given in Table I.

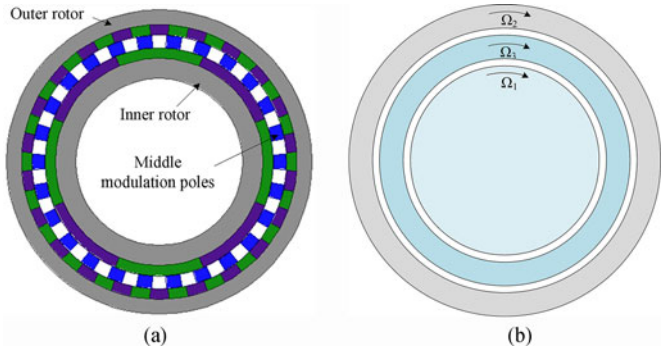

Fig. 5. Magnetic gear. (a) Construction. (b) Rotary parts of magnetic gear.

C. Working Principle

This torque split principle of the proposed DDF-PM machine is very important for the CR-PST system. In the following, this torque split principle is explained in detail. In the proposed DDF-PM machine, there exist bidirectional flux-modulation effects and synchronous rotation effect. The flux-modulation theory, which is originally applied to MGs, is shown in Fig. 5. In MGs, the flux-modulation poles serve to modulate the fundamental components of magnetic field to numbers of high-order harmonic components, which finally synchronize the low-speed rotor to produce a continuous positive thrust force. The rotating speed and pole pair numbers satisfy the following relationship [16], [17]:

$$p_1\Omega_1 + p_2\Omega_2 - p_3\Omega_3 = 0 \tag{1}$$

where p_1, p_2, p_3 represent the pole pair number of the inner rotor, outer rotor, and middle modulation pole pieces and $\Omega_1, \Omega_2, \Omega_3$ represent the rotating speeds of these three parts, respectively. The reference direction is shown in Fig. 5. From the equation, it is shown that when the middle rotor is stationary, the outer rotor's rotating speed is

$$\Omega_2 = -\frac{p_1\Omega_1}{p_2}. \tag{2}$$

Furthermore, if the inner rotor rotates in one direction and the middle rotor is rotating in the opposite direction, the outer rotor's rotating speed is expressed as

$$\Omega_2 = \frac{p_3\Omega_3 - p_1\Omega_1}{p_2}. \tag{3}$$

Since rotors rotate in the opposite direction, due to the angular relative velocity of the inner and middle rotor, the rotating speed of the outer rotor is increased compared to the case when the middle rotor is stationary. In a flux-modulation machine, the rotating magnetic field is produced by stator windings instead of rotating PMs. If PM rotors are replaced with stator windings, the rotating magnetic field and the winding frequency have the following relationship:

$$60f_i = p_i\Omega_i \qquad i = 1, 2, 3. \tag{4}$$

In order to achieve a stable torque and speed transmission, the pole-pair numbers of the stator windings, PMs, and modulation

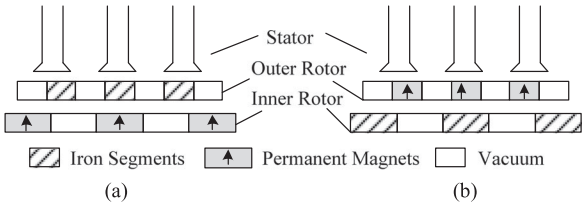

Fig. 6. Bidirectional flux-modulation effects. (a) Mode 1. (b) Mode 2.

poles need to satisfy the following relationship [16]–[18]:

$$n_m \pm p_w - p_{\mathrm{PM}} = 0 \tag{5}$$

where p_{PM} is the PM pole-pair number, n_m is the modulating pole number, and p_w is the stator winding pole-pair number. Subscript "*m*" and "*w*" represent modulation poles and winding.

In the proposed DDF-PM machine, there exist bidirectional flux-modulation effects. As shown in Fig. 6, modulation poles in the inner rotor serve to modulate the field excited by outer rotor PMs, denoted by Mode 1, while the modulation poles in the outer rotor can modulate the field excited by inner rotor PMs, as denoted by Mode 2. The resulted main components from the bidirectional modulation are the same, which is the 11th order harmonic component of magnetic flux. Consequently, the main winding is designed as $p_w = 11$.

For Mode 1, the pole number of modulating poles and PMs are n_{m_o} and p_{PM_i}, respectively. The pole pair numbers and rotational velocities of the inner rotor PM and outer rotor modulation poles satisfy the following relationships:

$$p_{\mathrm{PM}\_i} - n_{m\_o} + p_w = 0 \tag{6}$$

$$p_{\mathrm{PM}\_i}\Omega_{\mathrm{PM}\_i} - n_{m\_o}\Omega_{m\_o} + p_w\Omega_w = 0 \tag{7}$$

where Ω_{m_o} is the rotational velocity of the modulating poles, Ω_{PM_i} and Ω_w are the rotational velocities of the inner rotor PMs and the rotating speed of the field excited with stator winding, respectively.

Based on the law of energy conservation and under steady operation, one can obtain

$$T_{\mathrm{PM}\_i}\Omega_{\mathrm{PM}\_i} + T_{m\_o}\Omega_{m\_o} + T_{w1}\Omega_w = 0 \tag{8}$$

$$T_{\mathrm{PM}\_i} + T_{m\_o} + T_{w1} = 0 \tag{9}$$

where T_{PM_i}, T_{m_o}, and T_{w1} are the torque on the inner rotor PMs, out rotor modulating poles, and stator in Mode 1. From (6) to (9), the torque relationship can be expressed as

$$\begin{cases} T_{w1}/T_{\mathrm{PM}\_i} = p_w/p_{\mathrm{PM}\_i} \\ T_{m\_o}/T_{\mathrm{PM}\_i} = -n_{m\_o}/p_{\mathrm{PM}\_i} \end{cases}. \tag{10}$$

Similarly, for the Mod 2, the rotational velocities and torque satisfy the following relationship:

$$p_{\mathrm{PM}\_o} - n_{m\_i} - p_w = 0 \tag{11}$$

$$p_{\mathrm{PM}\_o}\Omega_{\mathrm{PM}\_o} - n_{m\_i}\Omega_{m\_i} - p_w\Omega_w = 0 \tag{12}$$

$$T_{\mathrm{PM}\_o}\Omega_{\mathrm{PM}\_o} + T_{m\_i}\Omega_{m\_i} + T_{w2}\Omega_w = 0 \tag{13}$$

$$T_{\mathrm{PM}\_o} + T_{m\_i} + T_{w2} = 0 \tag{14}$$

$$\begin{cases} T_{w1}/T_{\mathrm{PM}\_o} = p_w/p_{\mathrm{PM}\_o} \\ T_{m\_i}/T_{\mathrm{PM}\_o} = -n_{m\_i}/p_{\mathrm{PM}\_o} \end{cases} \tag{15}$$

where Ω_{m_i} and Ω_{PM_o} are the rotational velocities of the inner rotor modulation poles and outer rotor PMs. T_{PM_o}, T_{m_i}, and T_{w2} are the torque on the outer rotor PMs, inner rotor modulating poles, and stator in Mode 2. Since the velocities and pole numbers of modulation poles and PMs satisfy the following relationship:

$$\begin{cases} \Omega_{\mathrm{PM}\_o} = \Omega_{m\_o} \\ \Omega_{\mathrm{PM}\_i} = \Omega_{m\_i} \\ p_{\mathrm{PM}\_o} = p_{m\_o} \\ p_{\mathrm{PM}\_i} = p_{m\_i} \end{cases}. \tag{16}$$

Substitute (16) into (9) and (14), the torque and speed relationship can be derived as

$$T_{\mathrm{PM}\_i} + T_{m\_i} + T_{\mathrm{PM}\_o} + T_{m\_o} + T_{w1} + T_{w2} = 0 \tag{17}$$

$$\frac{T_{\mathrm{PM}\_i} + T_{m\_i}}{T_{\mathrm{PM}\_o} + T_{m\_o}} = -\frac{p_{\mathrm{PM}\_i}}{p_{\mathrm{PM}\_o}}. \tag{18}$$

The unified expression of the torque and speed relationship is expressed as

$$T_{i\_M} + T_{o\_M} = T_{w\_M} \tag{19}$$

$$G_r = \frac{T_{i\_M}}{T_{o\_M}} = -\frac{p_{\mathrm{PM}\_i}}{p_{\mathrm{PM}\_o}} \tag{20}$$

where $T_{o\_M} = T_{\mathrm{PM}\_o} + T_{m\_o}$, $T_{i\_M} = T_{\mathrm{PM}\_i} + T_{m\_i}$, and $T_{w\_M} = T_{w1} + T_{w2}$, which are the torque on the outer rotor, inner rotor, and stator with the excitation by the main winding and the subscript "*M*" refers to the main winding. The subscript "*o*," "*i,*" and "*w*" represent the out rotor, inner rotor, and winding, respectively.

In the proposed DDF-PM machine, there also exists a synchronous rotation effect. The auxiliary winding and outer rotor consist of a PMSM. The torque and pole pair of the auxiliary winding relationship satisfy the following equation:

$$T_{o\_A} = T_{w\_A} \tag{21}$$

$$p_{o\_A} = p_{w\_A} \tag{22}$$

where T_{o_A} and T_{w_A} are the torque on the outer rotor, and stator with the excitation by the auxiliary winding. p_{o_A} and p_{w_A} are the pole number of the outer rotor PM, and auxiliary stator winding with the excitation by only the auxiliary winding. The subscript "*A*" refers to the auxiliary winding. With the currents fed in both the main winding and the auxiliary winding, the total

torque on the outer rotor is expressed as

$$T_o = T_{o\_A} + T_{o\_M} \tag{23}$$

$$T_i = T_{i\_M}. \tag{24}$$

So, with the auxiliary winding, the newly derived torque ratio G_r' is not fixed but can be flexibly controlled with the main and auxiliary winding excitation. This can well explain the torque split principle of the proposed DDF-PM machine.

From (6) and (11), the unified velocity and pole pair relationship is expressed as

$$p_i - p_o + p_w = 0 \tag{25}$$

$$p_i\Omega_i - p_o\Omega_o + p_w\Omega_w = 0 \tag{26}$$

where Ω_i and Ω_o represent the rotational velocity of the inner rotor and outer rotor. p_i represents the pole number of inner rotor PM or modulation poles and p_o represents that of the outer rotor PM and modulation poles.

III. Wind Turbine Model and Its Simulation

Wind turbine's characteristics are the design basis of the CRPST system. In this paper, two Panasonic servo systems are used to simulate the main and auxiliary wind turbines. The wind turbine model and its simulation are discussed in this part.

A. Wind Turbine Model

According to the aerodynamic model of a wind turbine, the mechanical power P_m captured by the wind turbine from wind can be expressed as [19]

$$P_m = \frac{1}{2}\rho A_r {v_\omega}^3 C_p(\lambda, \beta) \tag{27}$$

in which ρ is the air density, A_r is the area swept by the wind blades, v_ω is the wind speed, C_p is the wind turbine power coefficient, which is related to the pith angle β and the blade tip speed ratio λ, which is defined by $\lambda = \frac{\omega_t R}{v_\omega}$, where ω_t is the wind turbine shaft speed and R is the radius of the wind turbine rotor plane.

For a single-rotor wind turbine, the maximum power that can be extracted from wind is expressed by

$$P_{\max} = \frac{1}{2}\rho A_r \frac{R^3 C_{p\max}}{\lambda_{\text{opt}}^3}\omega_t^3 = K_{\text{opt}}\omega_t^3 \tag{28}$$

where $C_{p\max}$ is the maximum wind turbine power coefficient, which is obtained when the tip-speed ratio is at its optimal value λ_{opt}. Then, the optimal torque of the wind turbine can be derived accordingly

$$T_{\text{opt}} = \frac{1}{2}\rho A_r \frac{R^3 C_{p\max}}{\lambda_{\text{opt}}^3}\omega_t^2 = K_{\text{opt}}\omega_t^2 \tag{29}$$

where K_{opt} is a constant determined by the wind turbine characteristics. The controller system controls the torque with the optimal reference torque signal obtained from (29), and the measured turbine shaft speed signal. Fig. 7 shows the typical wind turbine torque versus speed and power versus speed characteristics as well as the optimal power curve and torque curve for wind generation.

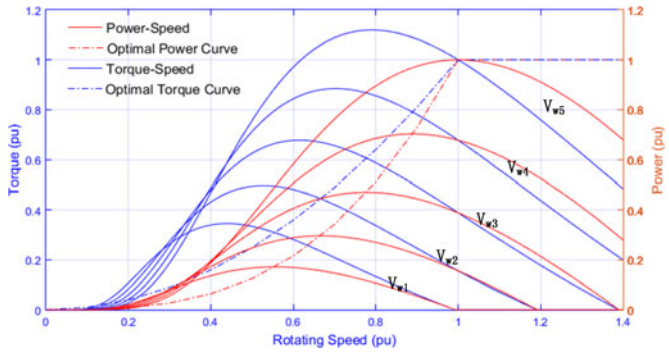

Fig. 7. Wind turbine torque-speed and power-speed characteristics.

MPPT control aims to adjust the machine to operate along the optimal reference torque curve, hence producing the maximum power at the given wind speed. The contra-rotating wind generation system has two wind turbines, and the blades and wind turbine characteristics are not the same. Dual MPPT control strategy should be developed to extract the maximum wind power.

Compared to a single-turbine wind power generator, the contra-rotating wind power generator has the following advantages:

1) A single-rotor wind generator always usually uses a gearbox to step up the slow turbine motion rotations to the faster generator rotations. While, this proposed dual-rotor wind generator is gearless and dual MPPT control can be directly used to modulate the rotation speed.
2) Previous research shows that a single rotor is more sensitive to the wind speed variations, since at an identical mechanical torque step change, the speed of the generator, which is connected to the single rotor, increases more than a dual rotor [20]. In addition to the better wind energy absorption of the dual-rotor system, the dynamic response of this system during the transient situation is more stable in comparison to the single-rotor system.
3) Due to the bidirectional flux-modulation effect, this proposed machine has improved torque density. Compared to the single-rotor machine in [21], the torque density is improved by around 20%.

B. Simulation of the Two Wind Turbines

CRWT system has two wind turbines. Both wind turbine power-speed working curves can be calculated by (27) and the OPT curve for each turbine can be calculated by (28). In our case, two Panasonic servo systems are used for simulating the main and auxiliary wind turbines, and the wind turbines working curves are calculated and scaled to fit the servo systems, as shown in Fig. 8. The dotted lines for the inner rotor simulate the auxiliary wind turbine and the solid lines for the outer rotor simulate the main wind turbine. The optimal speed/power/torque points of each curve are shown in Table II. These curves can be stored in the servo system and used to simulate the wind turbine

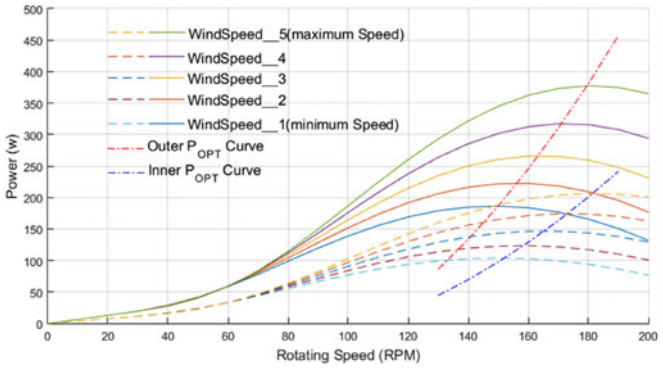

Fig. 8. Simulated wind turbine curves and the optimal power curve for each rotor.

TABLE II
SPECIFICATIONS OF THE SIMULATED WIND TURBINE CURVES

Wind speed curve No.		Optimal Speed (r/min)	Optimal Power (w)	Optimal Torque (N·m)
Inner Rotor	Curve 1	150	104	6.6
	Curve 2	160	123	7.4
	Curve 3	**170**	**146**	**8.2**
	Curve 4	170	174	9.8
	Curve 5	180	206	11.0
Outer Rotor	Curve 1	150	186	11.9
	Curve 2	160	222	13.3
	Curve 3	**160**	**266**	**15.9**
	Curve 4	170	317	17.8
	Curve 5	180	378	20.0

working condition. The bold one in the table is the curve used in the later experiments part.

IV. Control Strategy and Dual MPPT Control of Generation System

A. Dual d-q Coordination System

Since the stator auxiliary winding together with the outer rotor works as an ordinary PMSM machine, the control strategy of the auxiliary winding is the same as the traditional PMSM control. The main stator winding, outer rotor, and inner rotor combine a flux-modulation dual-rotor machine, the control of which is based on the resultant modulation flux control.

There are two *d*–*q*-axis coordination systems according to main winding and auxiliary winding in the stator as shown in Fig. 9. For the auxiliary winding, the *d*-*q*-axis system is located on the outer rotor, and *d*-axis is determined by the outer rotor PM field direction. For main windings, the *d*-*q*-axis system is located on the resultant modulation flux.

The synchronous speed formula $\Omega = 60$ f/p, and according to (26), the frequency relationship of the three parts are represented as

$$f_i - f_o + f_M = 0. \tag{30}$$

The electrical velocity can be expressed as $\omega = P \cdot \Omega$. Then, the electrical velocity relationship between the three parts is

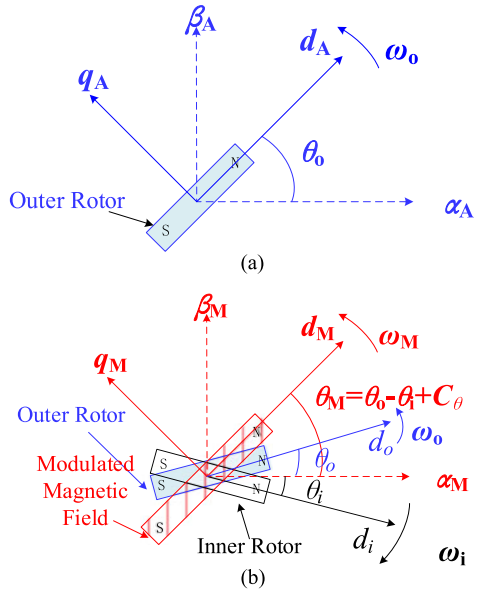

Fig. 9. Dual *d*-*q* coordination system. (a) Auxiliary windings. (b) Main windings.

derived accordingly

$$\omega_i - \omega_o + \omega_M = 0. \tag{31}$$

As $\omega = d\theta/dt$, the electrical angular position relationship can be derived

$$\theta_i - \theta_o + \theta_M = C_\theta \tag{32}$$

in which C_θ is a constant value. When α_M axis oriented flux in the main winding is assumed to be at the reference position, the value of C_θ is calculated as $C_\theta = -\theta_i - \theta_o$. For an auxiliary winding system, the angle θ_o between d_A and α_A in the coordination system are determined by the outer rotor position. For the main winding system, the angle θ_M between d_M and α_M in the coordination system is determined by both the outer and inner rotor positions, according to (31).

B. Mathematical Model of the DDF-PM Machine

The flux linkage equations of the proposed DDF-PM machine can be written as

$$\begin{bmatrix} \psi_{dM} \\ \psi_{qM} \\ \psi_{dA} \\ \psi_{qA} \end{bmatrix} = \begin{bmatrix} L_{dM} i d_M \\ L_{qM} i q_M \\ L_{dA} i_{dA} \\ L_{qA} i_{qE} \end{bmatrix} + \begin{bmatrix} \psi_M \\ 0 \\ \psi_o \\ 0 \end{bmatrix} \tag{33}$$

where, ψ_{dM}, ψ_{qM}, ψ_{dA}, ψ_{qA} are *d*- and *q*-axis flux linkage of the main and auxiliary windings, respectively; ψ_M is the resultant flux after the modulation by the inner and outer rotor; ψ_o is the flux of the outer rotor.

The voltage equations are written as follows:

$$\begin{bmatrix} u_{dM} \\ u_{qM} \\ u_{dA} \\ u_{qA} \end{bmatrix} = \begin{bmatrix} R_M i_{dM} \\ R_M i_{qM} \\ R_A i_{dA} \\ R_A i_{qA} \end{bmatrix} + p \begin{bmatrix} L_{dM} i_{dM} \\ L_{qM} i_{qM} \\ L_{dA} i_{dA} \\ L_{qA} i_{qA} \end{bmatrix} + \begin{bmatrix} -(\omega_o - \omega_i) L_{qM} i_{qM} \\ (\omega_o - \omega_i) L_{dM} i_{dM} \\ -\omega_o L_{qA} i_{qA} \\ \omega_o L_{dA} i_{dA} \end{bmatrix} + \begin{bmatrix} 0 \\ (\omega_o - \omega_i) \psi_M \\ 0 \\ \omega_o \psi_o \end{bmatrix} \tag{34}$$

where u_{dM}, u_{qM}, u_{dA}, u_{qA} are d- and q-axis voltages of the main and extra windings, respectively; R_M and R_A are the winding resistances of the main and auxiliary windings; p is the differential operator.

The torque on the inner and outer rotor is deduced as

$$\begin{bmatrix} T_i \\ T_o \end{bmatrix} = \frac{3}{2} \begin{bmatrix} -\dfrac{p_i}{p_o + p_i} p_M \psi_{qM} & \dfrac{p_i}{p_o + p_i} p_M \psi_{dM} & 0 & 0 \\ -\dfrac{p_o}{p_o + p_i} p_M \psi_{qM} & \dfrac{p_o}{p_o + p_i} p_M \psi_{dM} & -p_o \psi_{qA} & p_o \psi_{dA} \end{bmatrix} \begin{bmatrix} i_{dM} \\ i_{qM} \\ i_{dA} \\ i_{qA} \end{bmatrix}. \tag{35}$$

When $i_{\mathrm{d}} = 0$ control is used, the torque equation on the inner and outer rotors can be expressed as

$$\begin{bmatrix} T_i \\ T_o \end{bmatrix} = \frac{3}{2} \begin{bmatrix} \dfrac{p_i}{p_o + p_i} p_M \psi_M & 0 \\ \dfrac{p_o}{p_o + p_i} p_M \psi_M & p_o \psi_o \end{bmatrix} \begin{bmatrix} i_{qM} \\ i_{qA} \end{bmatrix}. \tag{36}$$

According to (36), it is shown that the shaft torque of the two rotors can be controlled separately, which is the basis for the dual MPPT control strategy and also agrees with the analysis in Section II-C.

C. Single MPPT With Only Main Winding Control

For comparison, single MPPT control with only main winding control is discussed in this part. The working condition is similar with the planetary gear system which gathers the mechanical power from CRWTs, and then transmits the mechanical power to the single-rotor generator, as proposed in [14]. The torque ratio with only the main winding is constant, so the torque split on the two shafts should follow a fixed gear ratio of p_i/p_o.

If there is no auxiliary winding, the torque equations are modified as

$$\begin{cases} T_i = \dfrac{3}{2} \dfrac{p_i}{p_o + p_i} p_M \psi_M i_{qM} \\ T_o = \dfrac{3}{2} \dfrac{p_o}{p_o + p_i} p_M \psi_M i_{qM} \end{cases} \tag{37}$$

which means the torque ratio of these two rotors should be fixed. However, in the MPPT control, with the speed feedbacks, the optimal torque references for these two rotors are determined according to the different optimal power curves, as shown in Fig. 8, and the torque relationship may conflict with this torque ratio.

Two possible operation situations may occur. Case 1 is according to the torque references, the calculated torque reference ratio $T_{i\_\mathrm{opt}}/T_{o\_\mathrm{opt}}$ is smaller than the gear ratio p_i/p_o. Then, i_{qM} command should be calculated according to (36)

$$i_{qM} = \frac{T_{i\_\mathrm{opt}}}{p_M \psi_M} \frac{2}{3} \frac{p_o + p_i}{p_i}. \tag{38}$$

Consequently, the inner rotor operates at the optimal operating point and the generated wind power is P_{i_opt}. However, the real torque on outer rotor is

$$T_o = \frac{p_o}{p_i} T_{i\_\mathrm{opt}} \tag{39}$$

which is smaller than the optimal torque reference T_{o_opt} from the optimal power curve. Then, on the main wind turbine, the absorbed wind energy P_{o} is smaller than P_{o_opt}.

Similarly, Case 2 refers to the opposite possibility, that the torque reference ratio T_{i_r}/T_{o_r} is greater than p_i/p_o. Then, the main wind turbine operates at the optimal operating point with the power output of P_{o_opt}, while the wind energy on the auxiliary wind turbine P_{i} would be smaller than the optimal power P_{i_opt}. With this method, only one wind turbine is guaranteed to operate at the optimal operation point.

In order to further improve the wind energy conversion efficiency, one can slightly adjust the i_{qM} command to maximize the total power generation $P_o + P_i$. A hill-climb search method is used to achieve this fine adjustment and hope to find the increased power output point. In this case, the i_{qM} commands should be increased to see whether the generation system can provide more power. Therefore, the increased i_{qM} commands would move the shaft with nonoptimal power output close to its optimal operating point, but move the previous shaft with optimal power output a little bit further from its optimal point. In the end, with this control strategy, both wind turbines would miss the optimal operation points and the total power generated is higher than that in Case 1 and Case 2. However, the final power generation is definitely smaller than $P_{o\_\mathrm{opt}} + P_{i\_\mathrm{opt}}$.

D. Dual MPPT With Both Winding Control Simultaneously

In this paper, a dual MPPT control strategy with two windings control simultaneously is used. From (36), it is shown that the inner rotor torque is only determined by the main windings, but the outer rotor torque is related to both the main and auxiliary windings.

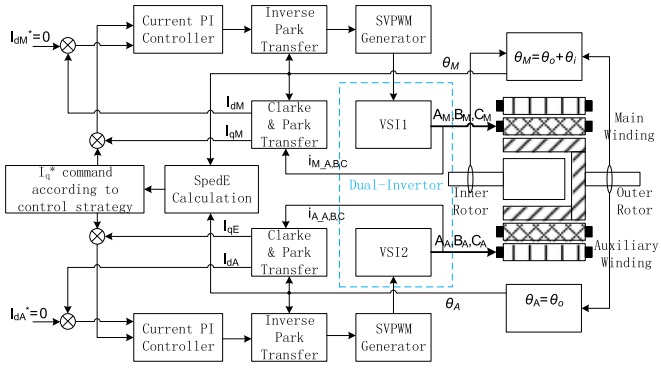

Fig. 10. Control diagram of the generation system.

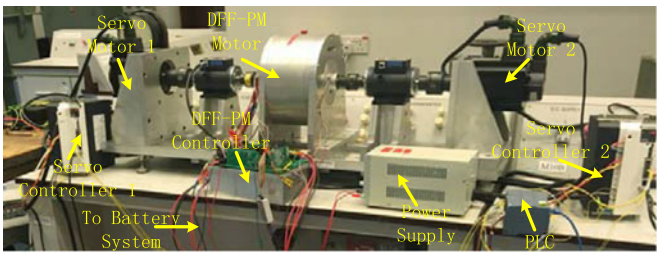

Fig. 11. Test bed.

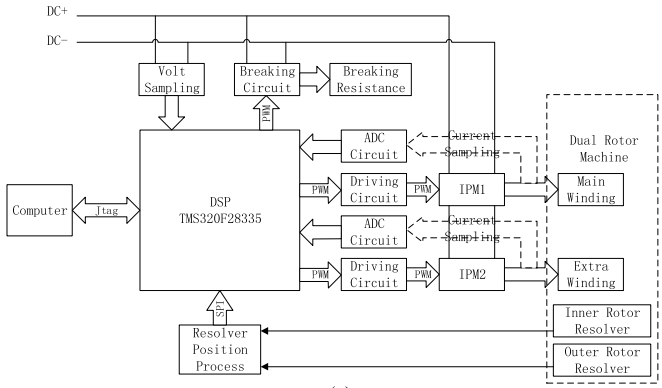

(a)

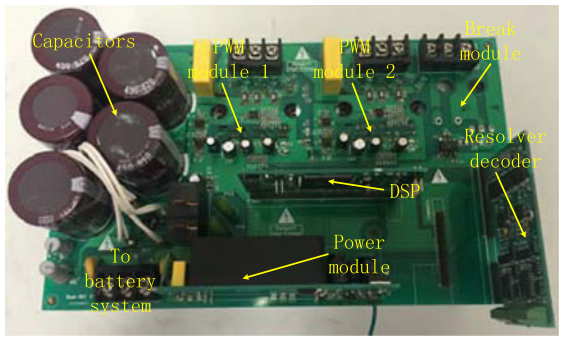

(b)

Fig. 12. Hardware implementation and photograph of the dual output controller. (a) Hardware implementation. (b) Photograph.

The control algorithm of the system is as shown in Fig. 10 and resolvers are installed in both rotors for position detection. According to (34), the outer rotor positions are used to control the torque of the outer rotor, and both rotor positions are used to control the torque of the inner rotor. Field-oriented control is applied on both the windings. When the reference torque value of the inner rotor is given, the main winding i_{qM} command can be determined with (36), and based on the fixed gear ratio, the corresponding torque on the outer rotor provided by the main winding can be obtained. Meanwhile, the auxiliary winding i_{qA} command is used for adjusting the outer rotor to chase its optimal torque reference value. The gap between the provided torque and the optimal torque reference on the outer rotor is filled by the auxiliary winding, and the value is $T_{o\_A} = 3/2 p_o \psi_o i_{q\,A}$. With this dual MPPT control strategy, the inner and outer rotor can both run at their own optimal operating points, and the maximum shaft powers can always reach $P_{o\_\mathrm{opt}} + P_{i\_\mathrm{opt}}$.

V. Simulation and Experiment Results

A. Experimental Setup

To verify the machine design and the control strategy, the test bed for the CR-PST system is shown in Fig. 11. The DDF-PM machine is located at the middle of the test bench, together with its dual VSI-based controller and dc power supply. A Panasonic 5 kw servo motor with its controller is connected to the outer rotor shaft to imitate the main wind turbine input. Meanwhile, a 3 kw servo motor system is connected with the inner rotor shaft and simulates the auxiliary wind turbine connection. A Siemens 1212C programmable logic controller (PLC), which stores the wind curves and wind turbine parameters, is used to control the two servo systems to simulate wind turbine under different winds. The CR-PST system is designed for charging 16 pieces of 12 V battery system.

Several wind curves are stored in the PLC and each curve corresponds to a specific wind speed. The servo systems output their shaft speeds to the PLC, and PLC gives the torque command back according to its storage wind curves and the real-time speeds. Different wind curves represent different wind speeds, and the same shaft speed will get different torque command according to different wind curves. In the dual MPPT experiments, five wind curves indicating five different wind speeds are stored in PLC.

B. Hardware Design for Controlling the Generator

To simultaneously control the two windings, a dual VSI-based controller with one digital signal processor (DSP, TMS320F28335) is designed. The hardware implementation of the dual output controller is as shown in Fig. 12.

As shown in Fig. 12, in controller one, DSP is designed as a card and plug in the main board. The inner and outer rotor position is detected by two resolvers, and their signals are decoded by the resolver-to-digital converter, which are transmitted by the serial peripheral interface. The DSP provides pulse width modulation signals to the two IPMs which are used to drive the two windings independently. The two IPMs share the same dc bus and the filter capacitors. A breaking system is also included in the controller for emergency situations.

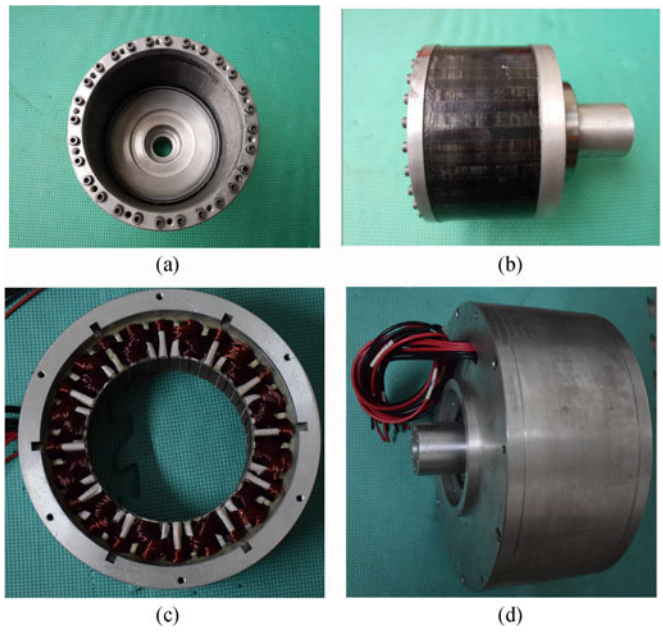

Fig. 13. Machine prototype and its components. (a) Middle rotor. (b) Inner rotor. (c) Stator. (d) The assembled machine prototype.

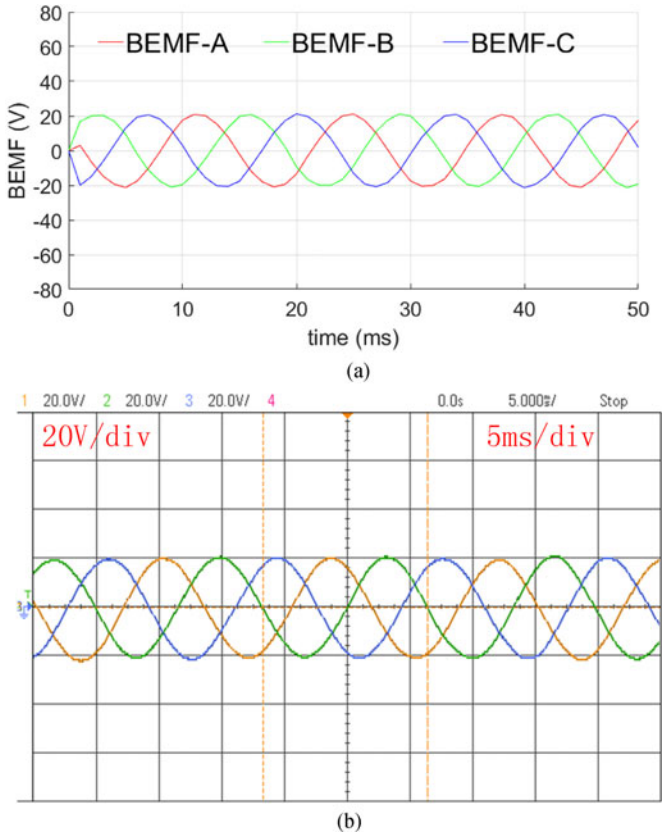

Fig. 14. Back EMF of the main windings with outer and inner rotor speed of 100 r/min. (a) Simulated results. (b) Experimental results.

C. Machine Design Verification

The prototype generator and its components are shown in Fig. 13. The back EMFs are shown in Figs. 14 and 15. The servos drive the two rotors to rotate at 100 r/min at opposite directions and the back EMFs of the three phases are recorded.

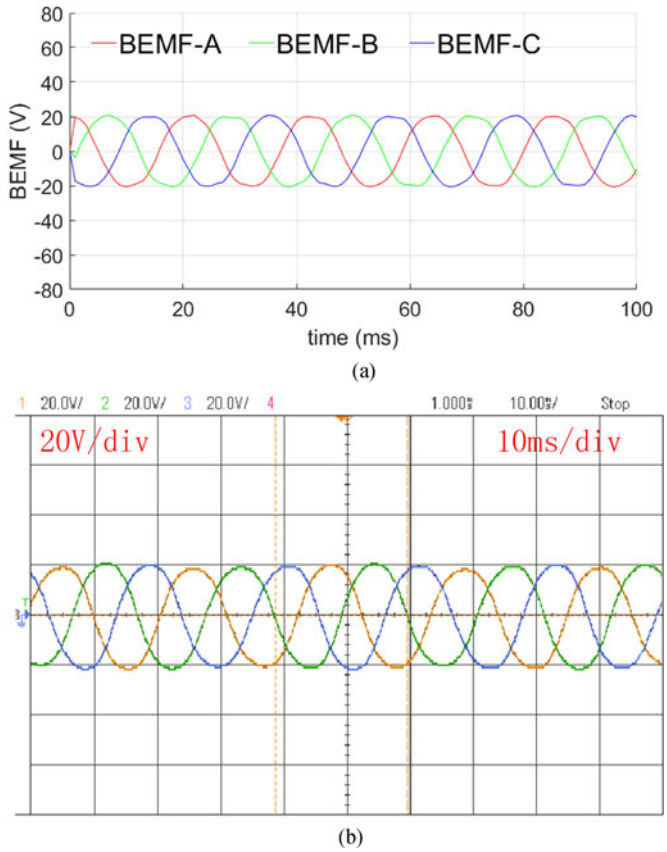

Fig. 15. Back EMF of the auxiliary windings with outer and inner rotor speed of 100 r/min. (a) Simulated results. (b) Experimental results.

These results agree well with the simulation results. The torque versus current waveforms can also be calculated and measured as shown in Fig. 16. The torque per ampere parameter characteristic directly affects the performance of the dual MPPT control, because the torque reference value can transfer to i_{q} command according to the curves.

Another precondition of the dual MPPT control is the separate torque control of the two rotors. The dynamic procedure experiment results are shown in Fig. 17. In Fig. 17, the rotors run at 100/–100 r/min condition, and lines represent inner rotor torque, outer rotor torque, main winding current, auxiliary winding current, respectively. At time T_1, the dynamic procedure starts, and the main winding current first increases linearly from zero, and then its peak value reaches 4.8 A at time T_2. The inner and outer rotor torque reaches 4.4 and 7.3 N·m, respectively. From T_2 to T_3, both winding currents are fixed, so that the torque is kept constant. Then, at time T_3, the auxiliary winding current increases linearly from zero and its peak value reaches 3 A at time T_4. From T_3 to T_4, the inner rotor torque is kept constant as the main winding current does not change. The outer rotor torque increases from 7.3 to 16 N·m as it is affected by the auxiliary winding current. Then the system keeps constant until time T_5. At the time T_5, the auxiliary winding current is reduced from 2.12 to −2.12 A linearly, as its i_{qA} command reduces gradually and finally goes opposite in sign. The outer rotor torque keeps going down until i_{qA} command reaches its opposite value. At

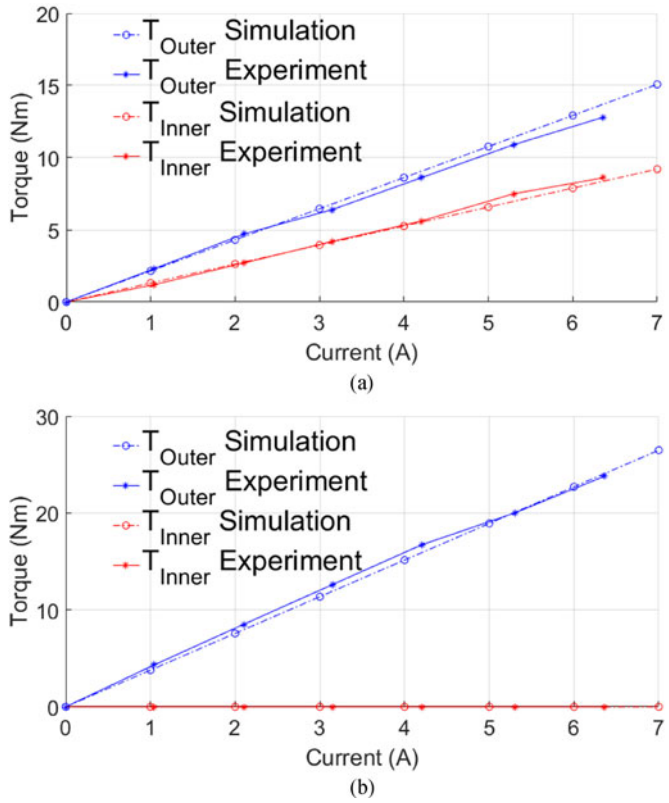

Fig. 16. Torque versus current waveforms. (a) The main winding. (b) The auxiliary winding.

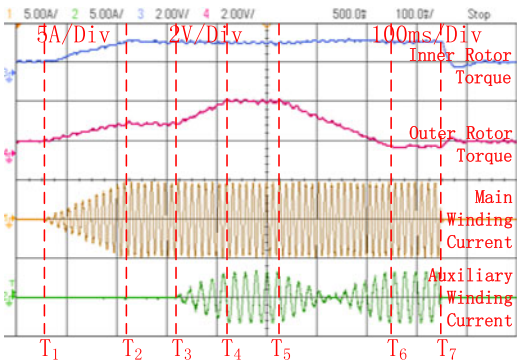

Fig. 17. Dynamic torque performance of the DDF-PM machine.

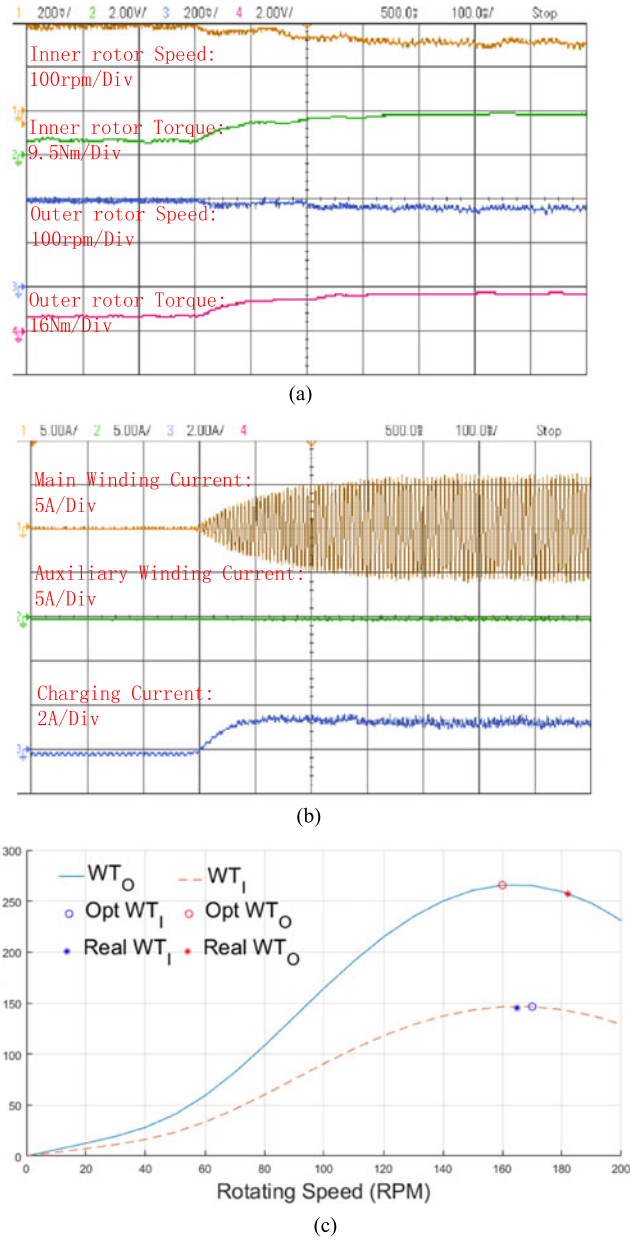

Fig. 18. MPPT with only main winding control. (a) Inner and outer rotor speed and torque. (b) The main and auxiliary winding current and charging current. (c) Simulated wind turbine curves for inner and outer rotor, with optimal working point and real working point.

time T_6, the auxiliary winding current amplitude is the same as that from T_4 to T_5, but the sign is opposite. The outer rotor torque reaches -1.5 N·m at time T_6. Finally, at time T_7, the system is shut down and both the torque goes to zero.

From the dynamic experiment above, a conclusion can be reached that torque on each rotors can be controlled separately, and the relationship of the torque and the current consists of the curves discussed in Fig. 16. Therefore, dual MPPT control then can be applied in this generation system with this flexible torque control.

D. Dual MPPT Control Experiments and Comparison

As mentioned in part A of this section, two servo motors, controlled by a PLC, are used to simulate the wind turbines. In the experiment, for each servo system, five wind curves stored with the command of PLC are as shown in Fig. 8, and the optimal point of these curves are as shown in Table II. In this experiment, there are seven parameters observed simultaneously with two oscilloscopes, namely inner rotor speed, inner rotor torque, outer rotor speed, outer rotor torque, main winding current, auxiliary winding current, and charging current. Fig. 18 shows the single MPPT strategy with only main winding control.

In Fig. 18, the wind turbine curves at wind speed_3 are used and the parameters at optimal points are shown in Table II, column one. As reference i_{qm} command calculated by the inner rotor optical torque curve is smaller than that calculated by the outer rotor curve, it is used as the controller command value.

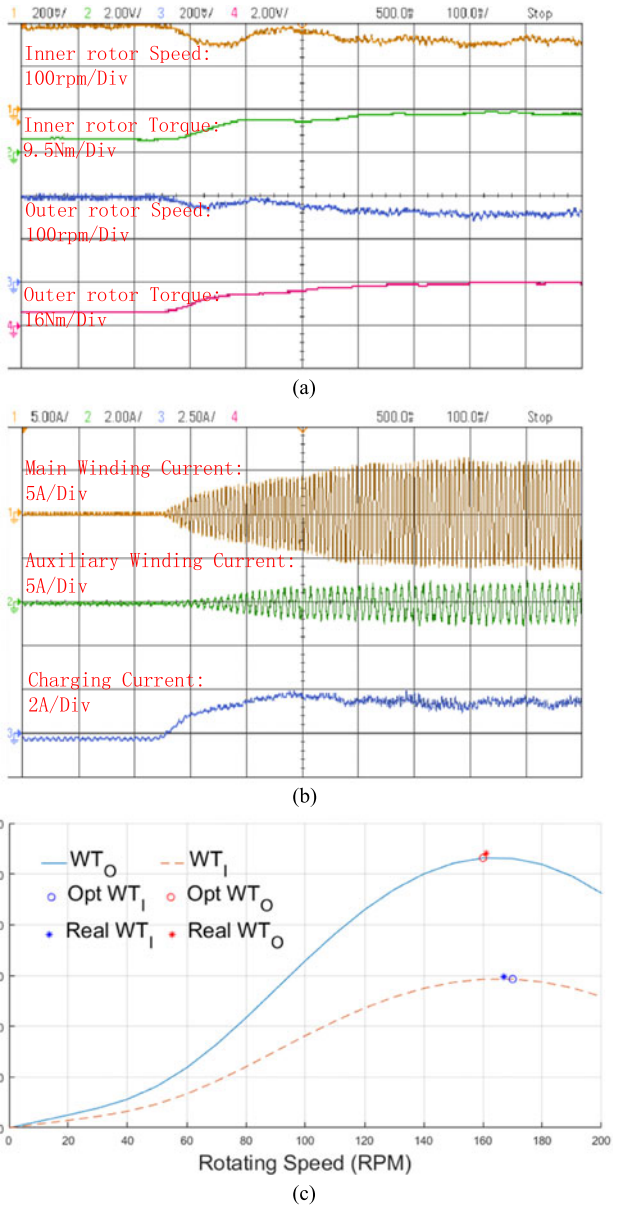

Fig. 19. Dual MPPT with two windings simultaneously control. (a) Inner and outer rotor speed and torque. (b) The main and auxiliary winding current and charging current. (c) Simulated wind turbine curves for inner and outer rotor, with optimal working point and real working point.

The inner wind turbine optimal speed from the optimal torque curve is 170 r/min and its corresponding torque reference is 8.2 N·m. The MPPT result is 165 r/min/8.4 N·m, which is very close to the optimal reference. However, at the same time, as the outer rotor does not run at its optimal point, its running speed is 182 r/min and torque is 13.5 N·m and the optimal point is 160 r/min/15.9 N·m.

The dual MPPT with both windings working simultaneously is shown in Fig. 19. The wind curves of the inner and outer rotors are both using curve 3, as the same as single MPPT control experiment. The control results are shown in Table III. The inner rotor's optimal value is 170 r/min, 8.2 N·m, and the outer rotor's optimal value is 160 r/min, 15.9 N·m. It can be seen from Fig. 19, the control results are 167 r/min, 8.5 N·m for inner rotor and 161 r/min, 16 N·m for outer rotor. Both rotors run at their optimal points, and in other words, both wind turbines run at their optimal power points. From Table III, the extracted power is increased by 14.3% with this dual MPPT control strategy compared with the single MPPT method. The experiments verify the effectiveness of the dual MPPT control strategy.

TABLE III
COMPARISON OF DIFFERENT MPPT PERFORMANCE

Parameters	Single MPPT	Dual MPPT
Inner Rotor Speed (r/min)	165	167
Inner Rotor Torque (N·m)	8.4	8.5
Outer Rotor Speed (r/min)	182	161
Outer Rotor Torque (N·m)	13.5	16
Main Winding Current (A)	4	4
Auxiliary Winding Current (A)	0	0.8
Battery System Voltage (V)	211	211
Charging Current (A)	1.4	1.6
Total mechanical Power (w)	400	415
Total electrical power (w)	295.4	337.6
Efficiency	73.9%	81.3%

VI. CONCLUSION

This paper proposes a new contra-rotating power spilt system for CRWT generation in which a doubly fed DDF-PM machine is used as the core element to efficiently absorb the wind energy. The structure is compact and the torque can be flexibly controlled with the main winding and the auxiliary winding. Compared with single MPPT with single stator winding control, dual MPPT control strategy can extract wind power energy with higher efficiency at the given wind speed. Simulation and experimental results verify the effectiveness of the proposed CR-PST system and the associated control strategy.

REFERENCES

[1] G. M. J. Herberta, S. Iniyanb, E. Sreevalsanc, and S. Rajapandiand, "A review of wind energy technologies," *Renewable Sustain. Energy Rev.*, vol. 11, no. 6, pp. 1117–1145, Aug. 2007.
[2] A. Thomas and L. Söder, "Wind energy technology and current status: A review," *Renewable Sustain. Energy Rev.*, vol. 4, no. 4, pp. 315–374, Dec. 2000.
[3] J. G. McGowan, A. L. Rogers, and J. F. Manwell, *Wind Energy Explained: Theory, Design and Application*, 2nd ed. Hoboken, NJ, USA: Wiley, 2009.
[4] P. S. Kumar, A. Abraham, R. J. Bensingh, and S. Ilangovan, "Computational and experimental analysis of a counter-rotating wind turbine system," *J. Sci. Ind. Res.*, vol. 72, pp. 300–306, 2013.
[5] H. M. McCoy, "Counter-rotating propellers," *Aeronaut. J.*, vol. 44, pp. 481–498, 1940.
[6] L. Seungmin, K. Hogeon, S. Eunkuk, and L. Soogab, "Effects of design parameters on aerodynamic performance of a counter-rotating wind turbine," *Renewable Energy*, vol. 42, pp. 140–144, 2012.
[7] L. Seungmin, K. Hogeon, and L. Soogab, "Analysis of aerodynamic characteristics on a counter-rotating wind turbine," *Curr. Appl. Phys.*, vol. 10, pp. S339–S342, 2010.
[8] J. D. Booker, P. H. Mellor, R. Wrobel, and D. Drury, "A compact, high efficiency contra-rotating generator suitable for wind turbines in the urban environment," *Renewable Energy*, vol. 35, pp. 2027–2033, 2010.
[9] W. Z. Shen, V. A. K. Zakkam, J. N. Sorensen, and K. Appa, "Analysis of counter-rotating wind turbines," *J. Phys.*, vol. 75, 2007, Art. no. 012003.

[10] S. Niu, S. L. Ho, and W. N. Fu, "A novel double-stator double-rotor brushless electrical continuously variable transmission system," *IEEE Trans. Magn.*, vol. 49, no. 7, pp. 3909–3912, Jul. 2013.
[11] C. Rossi, P. Corbelli, and G. Grandi, "W-CVT continuously variable transmission for wind energy conversion system," in *Proc. IEEE Power Electron. Mach. Wind Appl.*, 2009, pp. 1–10.
[12] Y. Liu, S. Niu, and W. N. Fu, "A novel multiphase brushless power-split transmission system for wind power generation," *IEEE Trans. Magn.*, vol. 52, no. 2, pp. 1–7, Feb. 2016.
[13] S. Niu, Y. Liu, S. L. Ho, and W. N. Fu, "Development of a novel brushless power split transmission system for wind power generation application," *IEEE Trans. Magn.*, vol. 50, no. 11, Nov. 2014, Art. ID: 8203004.
[14] S. N. Jung, T. No, and K. Ryu, "Aerodynamic performance prediction of a 30kW counter-rotating wind turbine system," *Renewable Energy*, vol. 30, pp. 631–644, 2005.
[15] J. M. Miller, "Hybrid electric vehicle propulsion system architectures of the e-CVT type," *IEEE Trans. Power Electron*, vol. 21, no. 3, pp. 756–767, 2006.
[16] K. Atallah, S. D. Calverley, and D. Howe, "Design, analysis and realisation of a high-performance magnetic gear," *IEE Proc. Elect. Power Appl.*, vol. 151, no. 2, pp. 135–143, Mar. 2004.
[17] Y. Chen, W. N. Fu, and W. Li, "Performance analysis of a novel triple-permanent-magnet- excited magnetic gear and its design method," *IEEE Trans. Magn.*, vol. 52, no. 7, pp. 1–4, Jul. 2016.
[18] S. Niu, S. L. Ho, W. N. Fu, and L. L. Wang, "Quantitative comparison of novel Vernier permanent magnet machines," *IEEE Trans. Magn.*, vol. 46, no. 6, pp. 2032–2035, Jun. 2010.
[19] Y. Zhao, C. Wei, Z. Zhang, and W. Qiao, "A review on position/speed sensorless control for permanent-magnet synchronous machine-based wind energy conversion systems," *IEEE J. Emerg. Sel. Topics Power Electron.*, vol. 1, no. 4, pp. 203–216, Dec. 2013.
[20] E. M. Farahani, N. Hosseinzadeh, and M. E. Mehran, "Comparison of dynamic responses of dual and single rotor wind turbines under transient conditions," in *Proc. IEEE Int. Conf. Sustain. Energy Technol.*, 2010, pp. 1–8.
[21] C. Liu, K. T. Chau, and Z. Zhang, "Novel design of double-stator single-rotor magnetic-geared machines," *IEEE Trans. Magn.*, vol. 48, no. 11, pp. 4180–4183, Nov. 2012.

Xiang Luo received the B.Sc., M.Sc., and Ph.D. degrees in electrical engineering from the School of Electrical Information and Electrical Engineering, Shanghai Jiao Tong University, Shanghai, China, in 2005, 2009, and 2013, respectively.

Since 2013, he has been with the Shanghai Jiao Tong University, where he is currently a Research Associate in the School of Electrical Information and Electrical Engineering. His research interests include electrical machines, motor drives for electric vehicles, renewable energy generation, and applied electromagnetics.

Shuangxia Niu (M'15) received the B.Sc. and M.Sc. degrees from the School of Electrical Engineering and Automation, Tianjin University, Tianjin, China, in 2002 and 2005, respectively, and the Ph.D. degree from the Department of Electrical and Electronic Engineering, The University of Hong Kong, Hong Kong, in 2009, all in electrical engineering.

Since 2009, she has been with The Hong Kong Polytechnic University, Kowloon, Hong Kong, where she is currently an Assistant Professor in the Department of Electrical Engineering. She has authored or coauthored more than 60 papers in leading journals. Her research interests include the design and control of novel electrical machines and drives, renewable energy conversion systems, and applied electromagnetics.